NUCL SCI TECH (2017) 28:53
DOI 10.1007/s41365-017-0196-9

Radar scattering width effects by coating $^{90}Sr/^{90}Y$ layers on cylindrical targets

Xiang Wang[1] · Jia-Zhu Zhu[1] · Wei Liu[1] · Chi Cui[1] · Rui-Li Zhang[1] · Fei Zhou[1] · Tao Tang[1] · Run-Sheng Huang[1]

Received: 29 January 2016 / Revised: 24 May 2016 / Accepted: 29 May 2016 / Published online: 1 March 2017

Abstract In this paper, the $^{90}Sr/^{90}Y$ coating effects on scattering width (SW) of cylindrical conductor targets are investigated. The electron density distribution of plasma around cylindrical targets of different radiuses is simulated under different radioactivities in normal or oblique incidence. In normal incidence, the SWs are examined as functions of frequency and scattering angle; while in oblique incidence, the SW is inspected as a function of incident angle at the frequency of 1.5 GHz. The results obtained are compared with those from an ideal perfect electric conductor (PEC) cylinder. It is demonstrated that the SW decreases over a wide frequency range in the back scattering region by coating a $^{90}Sr/^{90}Y$ layer on the cylindrical target. Moreover, the reduction in bi-static SW amplitude can reach 3–20 dB, when the incident angle is smaller than 30° at 1.5 GHz. It is a significant improvement in the stealth effect.

Keywords Radioactivity · Plasma · Cylinder · Scattering width (SW)

This work was supported by the 863 Program through the Ministry of Science and Technology (No. 2006AA03Z458) and the National Natural Science Foundation of China (Nos. 10904061 and 50977042).

✉ Run-Sheng Huang
rhuang@nju.edu.cn

[1] School of Physics, Nanjing University, Nanjing 210093, China

1 Introduction

Stealth effect to electromagnetic waves (EMW) is important for the survivability of weapon systems in battlefields and for military defense systems [1–3]. Since the bodies of aircraft cabins or missiles can be simplified as cylindrical objects, the study of EMW scattering from a cylindrical target has attracted considerable attention from researchers [4–11], and enhancing the stealth effects by coating new materials has become an attractive area of research [12–15]. As a type of specific absorbing materials, plasma coating is of significant EMW-absorption effect [16]. The scattering width (SW) of a cylindrical target can be greatly reduced by plasma coating.

Plasma can be induced by charged particles emitted from radioactive sources in the air. $^{90}Sr/^{90}Y$ is a perfect β-ray source. It emits no neutrons and ignorable γ-rays but just β-particles in maximum energy of 2.28 MeV and maximum trajectory range of 10 m in air [17–19]. In this paper, we investigate the absorption effect of plasma induced by $^{90}Sr/^{90}Y$ coating around a cylindrical target. The influences of $^{90}Sr/^{90}Y$ layer on mono-static and bi-static SWs of the cylindrical target at normal incidence are analyzed over the frequency range of 0.1–40 GHz, while the influences on bi-static SW at oblique incidence are analyzed at 1.5 GHz.

2 Theoretical background

2.1 Physical behavior of plasma induced by ^{90}Sr

As ^{90}Y is the decay product progeny of ^{90}Sr, we refer ^{90}Sr as $^{90}Sr/^{90}Y$. Figure 1 shows the continuous β spectrum

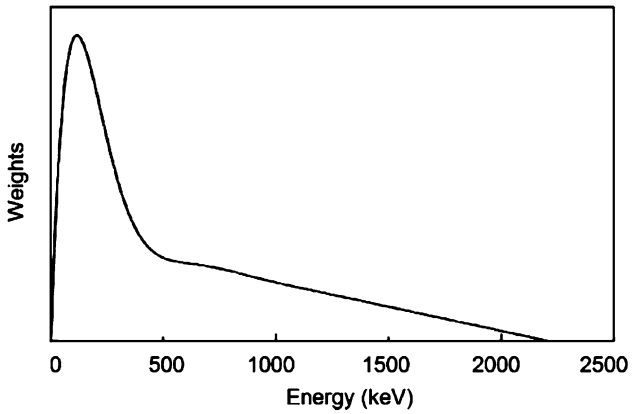

Fig. 1 Beta spectroscopy of ^{90}Sr

of ^{90}Sr [20]. The emitting directions and trajectories of β-particles from ^{90}Sr are all random, and the average values are obtained. The average energy losses of β-particles along the radial direction of a cylinder can be calculated. The average ionization energy of air molecules in atmosphere at normal temperature is 36 eV [21]. The average numbers of electron–ion pairs induced by one β-particle are simulated.

The emitted electrons diffuse in air [22, 23]. The number of electrons, N, passing through a unit area in a unit time is

$$\left(\frac{\mathrm{d}N}{\mathrm{d}t}\right)_{\mathrm{dif}} = -D_{\mathrm{dif}}\nabla n_{\mathrm{e}}, \tag{1}$$

where n_{e} is the electron density, and $D_{\mathrm{dif}} = 3.7 \times 10^2$ cm^2/s is the diffusion coefficient in air, as experimentally validated.

The electrons and positive ions are recombined after collision and the n_{e} changes in the recombination process as

$$\left(\frac{\mathrm{d}n_{\mathrm{e}}}{\mathrm{d}t}\right)_{\mathrm{rec}} \approx -\alpha n_{\mathrm{e}}^2, \tag{2}$$

where $\alpha = 1.5 \times 10^{-6}$ cm^3/s is the recombination coefficient, according to the experiments.

The electrons are absorbed by neutral particles as a result of collision, with the formation of negative ions, which can easily be photodetached by the sunshine. Considering the processes of ionization, diffusion, recombination, absorption and photolysis, the electron density (N_{m}) distribution in the plasma induced by β-particles from ^{90}Sr can be estimated. For un-magnetized plasma ($\mu_{\mathrm{r}} = 1$), the relative dielectric constant ε_{r} can be derived by

$$\varepsilon_{\mathrm{r}} = 1 - K_1\frac{\omega_{\mathrm{pe}}^2}{\omega_0^2 + v_{\mathrm{eff},l}^2} - jK_2\frac{v}{\omega_0}\frac{\omega_{\mathrm{pe}}^2}{\omega_0^2 + v_{\mathrm{eff},l}^2}, \tag{3}$$

where v, $v_{\mathrm{eff},\,l}$, and ω_{pe} are

$$v \sim v_{\mathrm{eff},l} \approx 1.5 \times 10^{11}\frac{N_{\mathrm{m}}}{2.7 \times 10^{19}}\sqrt{\frac{T}{300}}, \tag{4}$$

$$\omega_{\mathrm{pe}} = \sqrt{\frac{n_{\mathrm{e}}e^2}{m_{\mathrm{e}}\varepsilon_0}}, \tag{5}$$

and K_1 and K_2 are the coefficients related to the ratio of EMW frequency and the effective collision frequency [24].

2.2 Electromagnetic wave scattering from a cylindrical target

The cylindrical PEC target surrounded by inhomogeneous plasma can be simplified as a multilayered cylinder in the scattering problem. The geometry for an obliquely incident EMW is shown in Fig. 2a. The Z-axis coincides with the axis of the cylinder and X–Z is the incident plane. The tilt angle θ is the angle between the incident direction and the axis of the cylinder in the incident plane. Figure 2b shows cross section of the multilayered cylinder model. The plasma around the cylindrical target (of r_1 in radius) is divided into J layers, with r_j being the outer radius of the jth layer and m_j being its complex refractive index. The scattering angle φ is defined by the scattering direction and X-axis.

An eigenfunction expansion method is utilized to calculate the scattered filed for its relative simplicity in the situation of thick inhomogeneous layers coated cylinder. Based on Maxwell equations, the field in the jth layer can be written as [6, 9]

$$E_j = \sum_n (-1)^n\left[N_{n,j}^{(1)} - a_n^{(j)}N_{n,j}^{(3)} - ib_n^{(j)}M_{n,j}^{(3)}\right], \tag{6}$$

where M_n and N_n are eigenvectors. For transverse magnetic (TM) incident wave, the coefficients of the scattered field, a_n and b_n, can be expressed as [9]

$$\begin{aligned} a_n &= \frac{-ig_J\left(w_J^2 - 1\right)yn\cos\theta T_n(y)L_1}{y^2L_2L_3 - g_Jn^2\cos^2\theta(1 - w_J^2)} \\ b_n &= T_n(y)\cdot\frac{y^2L_3L_4 - g_Jn^2\cos^2\theta\left(1 - w_J^2\right)}{y^2L_2L_3 - g_Jn^2\cos^2\theta(1 - w_J^2)}, \end{aligned} \tag{7}$$

where $y = x_J\sin\theta, \eta_J = x_J\left(m_J^2 - \cos^2\theta\right)^{1/2}, w_J = y/\eta_J, g_J = \mu_J/m_J, h_J = m_Jy/\eta_J$, and $T_n(y) = J_n(y)/H_n^{(1)}(y)$. For the jth layer, $x_j = 2\pi r_j/\lambda$, with λ being wavelength of the incident EMW and μ_j being the plasma permeability in the jth layer. $L_{1\text{–}4}$ are as follows

$$\begin{aligned} L_1 &= D_n^{(1)}(y) - D_n^{(3)}(y), \quad L_2 = g_JD_n^{(3)}(y) - h_JH_n^{b(J)}, \\ L_3 &= D_n^{(3)}(y) - g_Jh_JH_n^{a(J)}, \quad L_4 = g_JD_n^{(1)}(y) - h_JH_n^{b(J)}, \end{aligned} \tag{8}$$

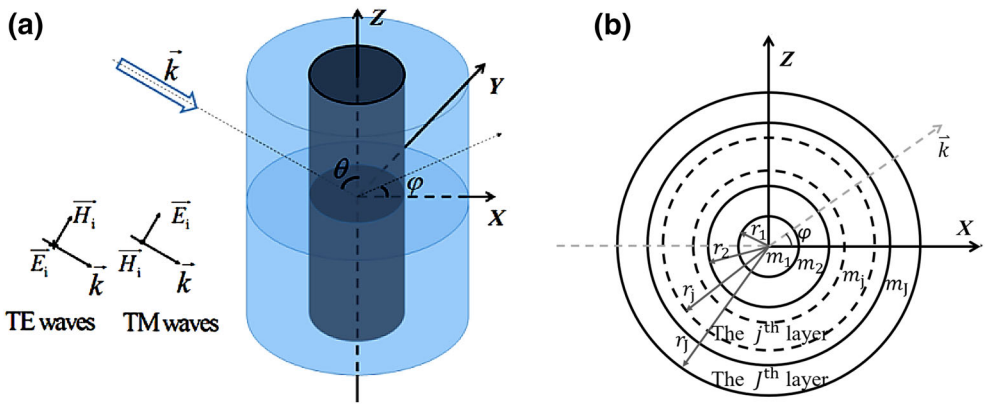

Fig. 2 Multilayered long cylinder model illuminated by EMW. **a** Geometry of scattering by infinite long inhomogeneous cylinders for oblique incidence; **b** Cross section of a multilayered cylindrical model

where $D_n^{(1)}(y) = J_n'(y)/J_n(y), D_n^{(2)}(y) = Y_n'(y)/Y_n(y)$ and $D_n^{(3)}(y) = H_n^{(1)'}(y)/H_n^{(1)}(y)$ are the logarithmic derivatives of the Bessel functions, that are used in computational calculation to overcome the overflow problems for high-order or large-argument cylindrical Bessel functions.

A recursive method is employed to get $H_n^{a(1)}$ and $H_n^{b(1)}$ [25] and expressed by the following recursive equations

$$
\begin{aligned}
A_n^{(j)} &= R_n^{(j)} \cdot \frac{\left[W_n^{a(j-1)} - D_n^{(1)}(\beta_{j-1})\right]}{\left[W_n^{a(j-1)} - D_n^{(2)}(\beta_{j-1})\right]} \\
B_n^{(j)} &= R_n^{(j)} \cdot \frac{\left[W_n^{b(j-1)} - D_n^{(1)}(\beta_{j-1})\right]}{\left[W_n^{b(j-1)} - D_n^{(1)}(\beta_{j-1})\right]} \\
H_n^{a(j)} &= \frac{D_n^{(1)}(\eta_j) - A_n^{(j)} D_n^{(2)}(\eta_j)}{1 - A_n^{(j)}} \\
H_n^{b(j)} &= \frac{D_n^{(1)}(\eta_j) - B_n^{(j)} D_n^{(2)}(\eta_j)}{1 - B_n^{(j)}} \\
W_n^{a(j)} &= \frac{\mu_j}{\mu_{j+1}} \left(\frac{\beta_j}{\eta_j} \cdot H_n^{a(j)} + \frac{n\lambda_j}{\mu_j \eta_j} \frac{\beta_j}{\eta_j} \right) \\
W_n^{b(j)} &= \frac{m_j^2}{m_{j+1}^2} \frac{\mu_{j+1}}{\mu_j} \left(\frac{\beta_j}{\eta_j} \cdot H_n^{b(j)} + \frac{n\lambda_j}{m_j^2} \frac{\mu_j}{\eta_j} \frac{\beta_j}{\eta_j} \right),
\end{aligned}
\tag{9}
$$

where $A_n^{(1)} = B_n^{(1)} = 0$ and $H_n^{a(1)} = H_n^{b(1)} = J_n'(\eta_j)/J_n(\eta_j)$ are initial values. $R_n^{(j)}$ is expressed as

$$
R_n^{(j)} = \left[J_n(\beta_{j-1}) \cdot Y_n(\eta_j)\right] / \left[Y_n(\beta_{j-1}) \cdot J_n(\eta_j)\right]. \tag{10}
$$

The $D_n^{(1)}(y)$, $T_n(y)$, and $R_n(y)$ functions are calculated with the following recursive relations

$$
\begin{aligned}
D_{n+1}^{(l)}(y) &= -\frac{n+1}{\rho} + \frac{1}{n/\rho - D_n^{(l)}(y)}, l = 1, 2, 3. \\
T_n(y) &= T_{n-1}(y) \cdot \frac{D_n^{(3)}(y) + n/\rho}{D_n^{(1)}(y) + n/\rho} \\
R_n^j(y) &= R_{n-1}^j \cdot \frac{D_n^{(2)}(\beta_{j-1}) + n/\beta_{j-1}}{D_n^{(1)}(\beta_{j-1}) + n/\beta_{j-1}} \cdot \frac{D_n^{(1)}(\eta_j) + n/\eta_j}{D_n^{(2)}(\eta_j) + n/\eta_j},
\end{aligned}
\tag{11}
$$

where $D_n^{(1)}(y)$ is evaluated using a downward recurrence formula. The initial value for the downward recurrence formula is generated using the method provided by Lentz [26]. The remaining four functions are computed using the upward recurrence formulas with initial values obtained from Matlab programs.

The electric field can be divided into incident part E_i and scattered part E_s. So, the SW is defined as

$$
\sigma = \lim_{\rho \to \infty} \left[2\pi\rho \frac{|E_s|^2}{|E_i|^2} \right]. \tag{12}
$$

The relationship between σ and the scattering coefficients is

$$
\sigma = \lim_{\rho \to \infty} [2\pi\rho(I_1 + I_2)]. \tag{13}
$$

For TM waves

$$
\begin{aligned}
I_1 &= \frac{2}{k_0 \pi r} \left| b_0 + 2 \sum_{n=1}^{\infty} b_n \cos(n\varphi) \right|^2 \\
I_2 &= \frac{2}{k_0 \pi r} \left| 2 \sum_{n=1}^{\infty} a_n \sin(n\varphi) \right|^2.
\end{aligned}
\tag{14}
$$

For transverse electric (TE) waves, the coefficients of the scattered field, a_n and b_n, are [9]

$$a_n = T_n(y) \cdot \frac{y^2 L_5 L_2 - g_J n^2 \cos^2\theta(1-w_J^2)}{y^2 L_2 L_3 - g_J n^2 \cos^2\theta(1-w_J^2)}$$
$$b_n = \frac{-ig_J(w_J^2-1)yn\cos\theta T_n(y) L_1}{y^2 L_2 L_3 - g_J n^2 \cos^2\theta(1-w_J^2)}, \quad (15)$$

where

$$L_5 = \frac{J_n'(y)}{J_n(y)} - g_J h_J H_n^{a(J)}, \quad (16)$$

and

$$I_1 = \frac{2}{k_0\pi r}\left|a_0 + 2\sum_{n=1}^{\infty} a_n \cos(n\varphi)\right|^2$$
$$I_2 = \frac{2}{k_0\pi r}\left|2\sum_{n=1}^{\infty} b_n \sin(n\varphi)\right|^2. \quad (17)$$

All the SW values provided in the following sections are represented in normalized form, 10 lg(σ/λ).

2.3 Validation of the algorithm at high frequency

Accuracy of the eigenfunction expansion method used in this work has always been doubted when the size parameter is of high value ($x_j = 2\pi r_j/\lambda$) [27]. We compare the results of this algorithm with those of an asymptotic solution [28] for SWs of a dielectric layer-coated PEC cylinder in the TM case, as shown in Fig. 3. The cylinder radius is 10 m and the layer is 0.08 m thick. The results of the eigenfunction expansion method and the geometrical optics solution (GO, an asymptotic solution in deep lit region) agree well at 40 GHz and $\varphi > 90°$, but are deviating from each other with decreasing frequencies, just because that the GO solution appears to be too simple for the issue. We note that for the TE case the two kinds of results are similar (not shown). Therefore, the calculation results of this work with $r_J = 10$ m can be reliable at high frequencies.

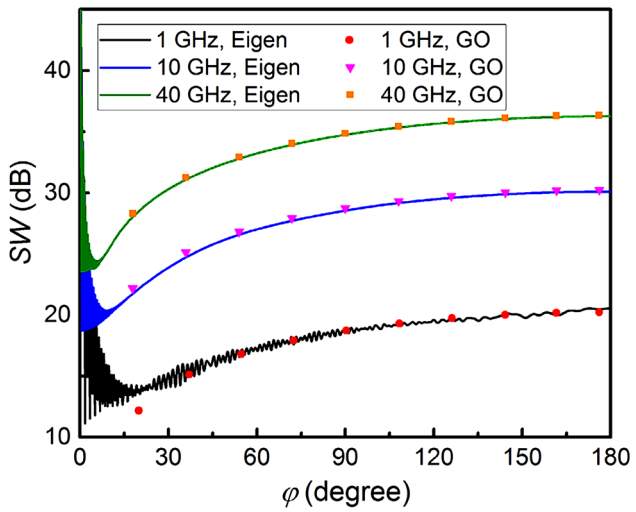

Fig. 3 SWs calculated with the eigenfunction expansion method (eigen), and the asymptotic solution (GO). The relative dielectric constants of the coated layer are $0.9994 - 0.16i$, $0.9995 - 0.0014i$ and $0.9998 - 0.00012i$ at 1, 10 and 40 GHz, respectively, with the relative permeability of 1

The inaccuracy in the eigenfunction expansion results mainly originates from bad convergence of the Bessel functions with large arguments. However, as logarithmic derivatives of the Bessel functions have replaced the Bessel functions, the recursive relations with reliable initial values have enabled us to obtain numerical values with higher orders, thereby the coefficients (a_n and b_n) can be truncated as tiny as 10^{-15} in the calculation, so as to ensure accuracy of the results. The truncation order for relatively high frequency is provided in Sect. 3.

Asymptotic solutions have been widely recognized in high frequency EMW scattering problems, but their complicity increases with the number and thickness of the coating layers. Here, the plasma around the cylinder is of 8 m thickness, divided into 100 layers. Thus, eigenfunction expansion is the right method for its unified form in the multilayer situation.

3 Results and discussion

3.1 Electron density distribution of the plasma

Figure 4 shows electron density distribution of the plasma induced by β-particles from the ^{90}Sr coating in radioactivity of 1 and 10 Ci/cm^2, assuming a long cylinder in radiuses of 0.5 and 2 m, respectively. For the cylinder of 0.5 m radius, at 1 Ci/

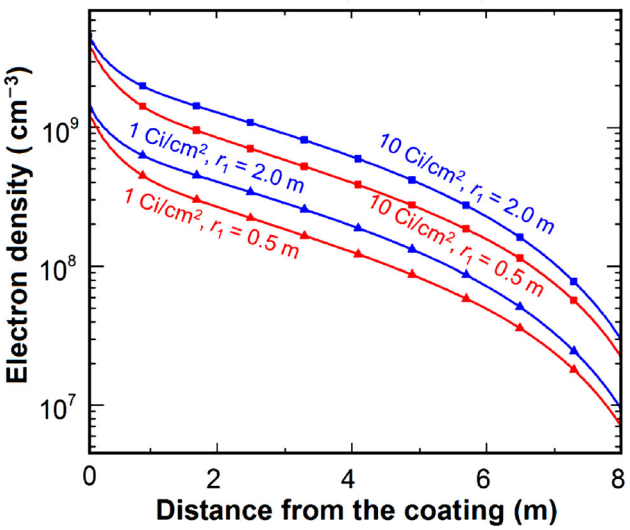

Fig. 4 Electron density distribution of the plasma excited by the ^{90}Sr coating

cm^2, the electron density of the plasma is 1.56×10^9 cm^{-3} adjacent to the ^{90}Sr coating, while it is 6.89×10^6 cm^{-3} at 8 m from the coating. As the amount of electron–ion pairs in a unit time increases with the radioactivity, the electron density of the plasma increases accordingly [24]. At 10 Ci/cm^2, the corresponding electron densities are 4.95×10^9 and 2.18×10^7 cm^{-3}, respectively. Compared to the maximum value, the electron densities are reduced by two orders of magnitude at 8 m from the ^{90}Sr coating for both radioactivities. The plasma around the cylinder of 2 m radius yields greater electron density at the same radioactivity and distance, while similar density-decreasing behavior with increasing distance up to 8 m. Therefore, the influence of plasma on the EMW propagation at 8 m from the ^{90}Sr coating can be ignored and 8 m is set as the thickness of the plasma surrounding the cylinder target in the calculation.

3.2 The mono-static SW

In order to clearly differentiate between the SWs of coated and uncoated cylindrical targets, the reduction of SW is used to display the data

$$d_{SW} = SW_{\text{with } ^{90}Sr \text{ coating}} - SW_{\text{without } ^{90}Sr \text{ coating}}. \quad (18)$$

The mono-static d_{SW}s of the ^{90}Sr-coated cylindrical targets ($r_1 = 0.5$ and 2 m) verses EMW frequency (0.1–40 GHz) at normal incidence are illustrated in Fig. 5. The insets show the SWs by the corresponding cylinders made with PEC. The mono-static SW by a PEC cylinder increases smoothly with the EMW frequency for TM waves and alternates for TE waves. The oscillations in the TE case arise from the creeping waves of TE polarization. In the backscattering region (from $\varphi = 90°$ to $\varphi = 180°$), the scattered waves are composed of creeping and reflected waves for TE polarization, but mainly reflected waves for TM polarization, and the phase difference between the two waves changes significantly with the EMW frequency [29, 30]. The SW by the ^{90}Sr-coated cylindrical target decreases remarkably as the EMW energy is absorbed by the plasma. For the target of 0.5 m radius, the mono-static SW decreases over 0.85 dB at the radioactivity of 1 Ci/cm^2 in the frequency range of 0.5–7 GHz and more than 2.80 dB at 10 Ci/cm^2 in 0.8–4 GHz. The full width at half maximum (FWHM) of all d_{SW} curves can reach 27 GHz. Having the greater plasma density, the mono-static SWs of the ^{90}Sr-coated target of 2 m radius decreased more than those in the 0.5 m case, by 1.25 dB at 1 Ci/cm^2 in 0.6–6 GHz and 3.95 dB at 10 Ci/cm^2 in 0.6–4 GHz. In addition, the FWHM can also reach 27 GHz.

The truncation orders against the frequency in the TM case are shown in Fig. 6. The orders for different radioactivities are close to each other for cylinders of the same radius, while they increase with the radius, but the increment is not large as the cylinder radius is much smaller than the surrounded plasma thickness. The orders for both radiuses increase linearly with the frequency, reaching 7245 for 0.5 m radius and 8534 for 2.0 m radius. The truncation order is mainly determined by the size parameter x_J [31], and it can be predicted that it shall not exceed 20,000 at 100 GHz for a cylinder of 2 m radius. The truncation orders in the TE case are identical to the TM results.

3.3 The bi-static SW at normal incidence

The bi-static SWs of the cylindrical target ($r_1 = 0.5$ m) with and without the ^{90}Sr coating for the EMW at normal incidence are calculated in the frequency range of 0.1–40 GHz. The data are displayed in 2D images with scaled colors, as shown in Fig. 7. For TM waves, the bi-static SW by a PEC cylinder increases steadily with the frequency and scattering angle in the back scattering region (Fig. 7a). However, it gets complicated in the forward scattering region (from $\varphi = 0°$ to $\varphi = 90°$). The reason is that several modes of the EMW rays are involved in that scattered filed. Similar phenomenon is observed in the TE case (Fig. 7c). After the PEC cylinder is coated with a 10 Ci/cm^2 ^{90}Sr layer, SW by the scatter decreases significantly in the back scattering region (Fig. 7b). Comparing

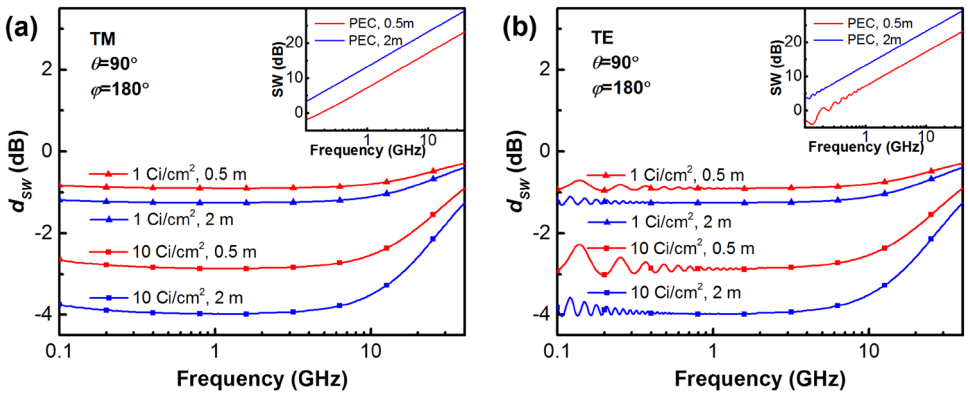

Fig. 5 Mono-static d_{SW}s of the cylindrical target with ^{90}Sr coating. **a** TM waves; **b** TE waves

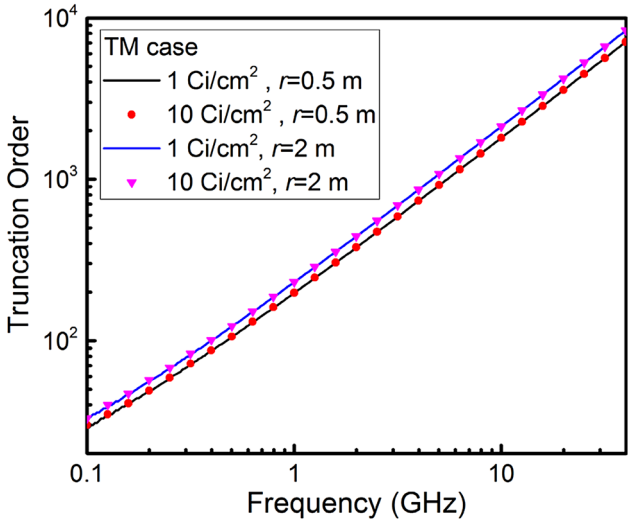

Fig. 6 Truncation orders in the calculation. I_1 and I_2 in Eqs. (14) and (15) are truncated when $b_n \leq 10^{-15}$ and $a_n \leq 10^{-15}$

Fig. 7b, d, the ^{90}Sr reduction effects in the TE and TM cases are similar.

The bi-static d_{SW}s of the 10 Ci/cm^2 ^{90}Sr-coated cylinder are investigated as functions of scattering angle φ at four typical EMW frequencies: 0.2, 1.5, 27, and 40 GHz, as shown in Fig. 8. For TM waves, the d_{SW}s increase slightly with the scattering angle in the back scattering region. The d_{SW}s at $\varphi = 90°$ are −2.87, −3.06, −1.54 and −0.96 dB, for 0.2, 1.5, 27 and 40 GHz, respectively. For TE waves, the d_{SW}s show a similar trend but with more intense oscillations, especially at low frequencies, which can also be attributed to the phase difference between the creeping and reflected waves.

3.4 The bi-static SW at oblique incidence

Bi-static SWs are calculated with obliquely incident EMWs at 1.5 GHz and the cylinder of 0.5 m radius, with and without ^{90}Sr coating (10 Ci/cm^2), in the back scattering region in incident angles of $0° < \theta < 90°$, as depicted in Fig. 9. For TM waves, the SW by the PEC cylinder does not change with the incident angle θ, while the SW by the ^{90}Sr-coated one decreases remarkably with θ. The reason is that the propagation distance of the EMW in the plasma increases with decreasing incident angles. For TE waves, the SW by the PEC cylinder oscillates with the changes in θ and φ due to the creeping waves, while the SW by the coated one shows a downward trend for small incident angles ($\theta < 50°$), similar to that in the TM case.

The bi-static d_{SW}s of the 10 Ci/cm^2 ^{90}Sr-coated cylindrical target are studied as functions of θ at three typical

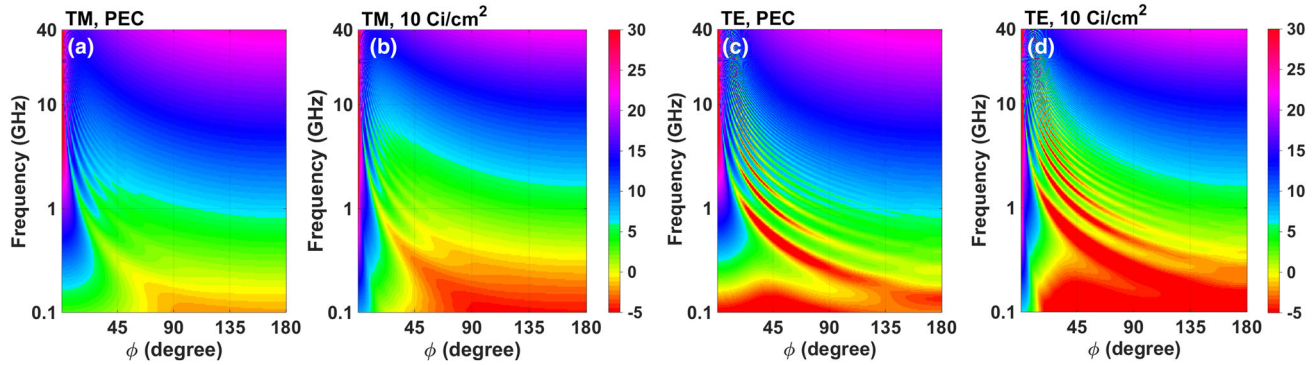

Fig. 7 Bi-static SWs of the cylindrical target at normal incidence. **a** TM, PEC; **b** TM, 10 Ci/cm^2; **c** TE, PEC; **d** TE, 10 Ci/cm^2

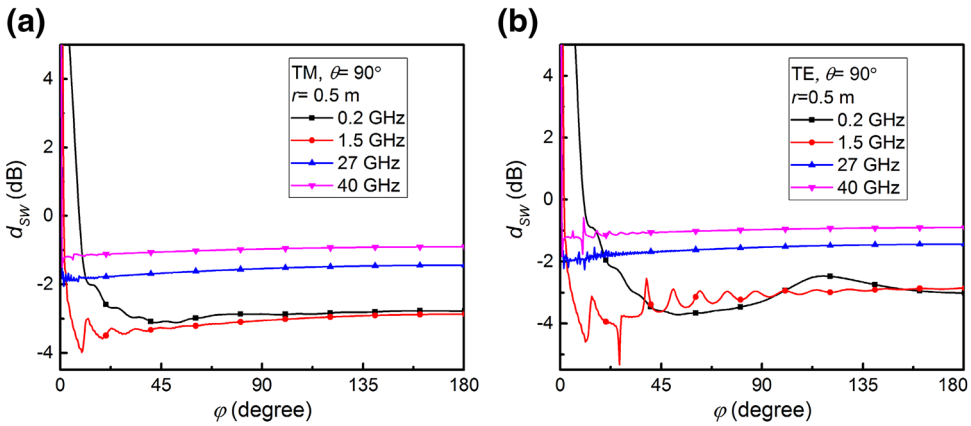

Fig. 8 Bi-static d_{SW}s of the cylindrical target coated with ^{90}Sr layer at normal incidence. **a** TM waves; **b** TE waves

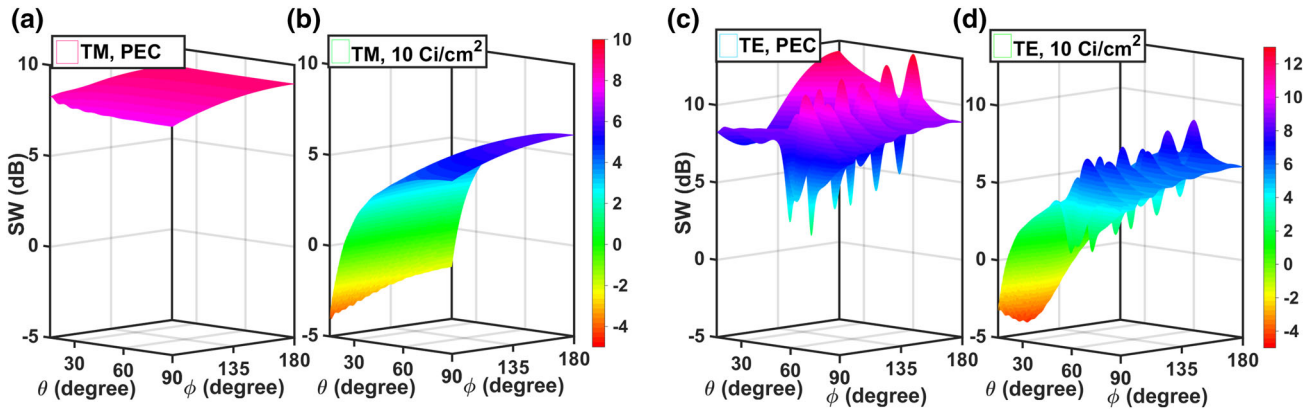

Fig. 9 Bi-static SWs at oblique incidence. **a** TM, PEC; **b** TM, 10 Ci/cm^2; **c** TE, PEC; **d** TE, 10 Ci/cm^2

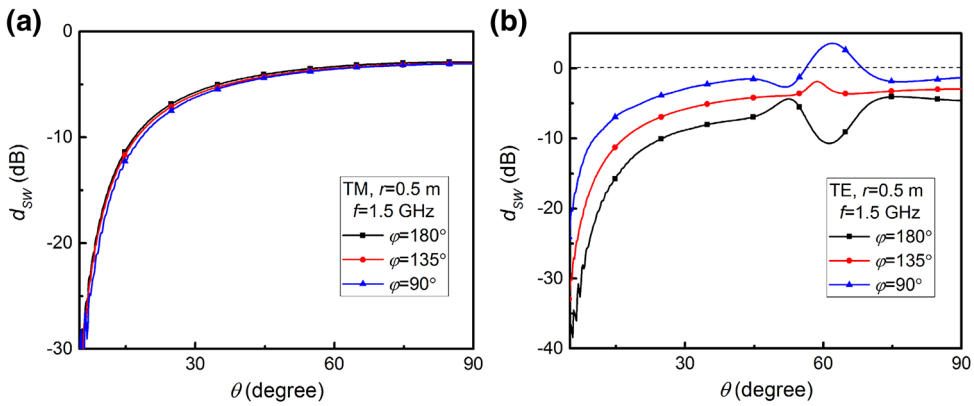

Fig. 10 Bi-static d_{SW}s of the ^{90}Sr-coated cylindrical target at typical incident angles at 10 Ci/cm^2 for TM waves (**a**) and TE waves (**b**)

scattering angles: 180°, 135°, and 90°, as shown in Fig. 10. The EMW frequency is 1.5 GHz. For TM waves, the d_{SW}s of the 10 Ci/cm^2 ^{90}Sr-coated cylinder decrease with θ and display close values for different scattering angles. The d_{SW}s reach -5 to -30 dB when $\theta < 30°$. For TE waves, the d_{SW}s decrease with θ in most of the incident angles but oscillate in the range of $55° < \theta < 75°$, which can also be attributed to the creeping waves. Moreover, the d_{SW}s for different scattering angles are no longer close to each other. When $\theta < 30°$, the d_{SW}s reach -9 to -38, -6 to -31 and -3 to -20 dB at $\theta = 180°$, 135° and 90°, respectively.

4 Conclusion

In this paper, influences of ^{90}Sr coating on electromagnetic scattering from a cylindrical target are investigated and evaluated. The results demonstrate that the SW of a cylindrical target with ^{90}Sr coating decreases effectively. The mono-static SW by the 10 Ci/cm^2 ^{90}Sr-coated cylindrical target reduces by 2.80 and 3.95 dB for 0.5 and 2 m radiuses, respectively, in the frequency range of 0.4–40 GHz. The bi-static SWs by 10 Ci/cm^2 ^{90}Sr-coated cylindrical target of 0.5 m radius at normal incidence reduce by 2.87, 3.06, 1.54, and 0.96 dB in the back scattering region, for EMW frequencies of 0.2, 1.5, 27, and 40 GHz, respectively. In addition, the stealth effect can be significantly improved for oblique incidence of EMWs. The bi-static SW by the cylindrical target with 10 Ci/cm^2 ^{90}Sr coating reduces by 3–20 dB when the incident angle θ is smaller than 30°. The results indicate that ^{90}Sr-coated cylindrical objects have significant stealth effect.

References

1. G.X. Wu, S. Liu, S.Y. Zhong, Numerical analysis of propagation characteristics of electromagnetic wave in lossy left-handed material media. Optik **125**, 4233–4237 (2014). doi:10.1016/j.ijleo.2014.04.018
2. S. Shen, M. Chung, FDTD simulations on radar cross sections of metal cone and plasma covered metal cone. Vacuum **86**, 970–984 (2012). doi:10.1016/j.vacuum.2011.08.016
3. B.P. Li, C.G. Wang, W. Wang et al., Electromagnetic wave absorption properties of composites with micro-sized magnetic particles dispersed in amorphous carbon. J. Magn. Magn. Mater. **365**, 40–44 (2014). doi:10.1016/j.jmmm.2014.01.015
4. R.X. Lord, On the electromagnetic theory of light. Philos. Mag. **12**, 81–101 (1881). doi:10.1080/14786448108627074
5. J.R. Wait, Scattering of a plane wave from a circular dielectric cylinder at oblique incidence. Can. J. Phys. **33**, 189–195 (1955). doi:10.1139/p55-024

6. C.F. Bohren, D.R. Huffman, *Absorbing and Scattering of Light by Small Particles* (Wiley, New York, 1983), pp. 194–199
7. M. Barabas, Scattering of a plane wave by a radially stratified tilted cylinder. Opt. Soc. Am. A **4**, 2240–2248 (1987). doi:10.1364/JOSAA.4.002240
8. Z.S. Wu, Y.P. Wang, Electromagnetic scattering for multilayered sphere-recursive algorithms. Radio Sci. **26**, 1393–1401 (1991). doi:10.1029/91RS01192
9. N. Gurwich, M. Shiloah, Klerman, The recursive algorithm for electromagnetic scattering by tilted infinite circular multilayered cylinder. J. Quant. Spectrosc. Radiat. **63**, 217–229 (1999). doi:10.1016/S0022-4073(99)00017-5
10. H.F. Jiang, X.E. Han, R.X. Li, Improved algorithm for electromagnetic scattering of plane waves by a radially stratified tilted cylinder and its application. Opt. Commun. **266**, 13–18 (2006). doi:10.1016/j.optcom.2006.04.041
11. N. Iqbal, P.K. Choudhury, P.S. Menon, Scattering from silver metal cylinder due to L-nihility coated with conducting sheath helix embedded dielectric medium. J. Electromagn. Waves **29**(10), 1354–1374 (2015). doi:10.1080/09205071.2015.1044128
12. R. Paknys, N. Wang, Creeping wave propagation constants and modal impedance for a dielectric coated cylinder. IEEE Trans. **34**, 674–680 (1986). doi:10.1109/TAP.1986.1143865
13. J. Sun, W. Sun, Directive electromagnetic radiation of a line source scattered by a conducting cylinder coated with left-handed metamaterial. Microw. Opt. Technol. Lett. **47**(3), 274–279 (2005). doi:10.1002/mop.21145
14. S. Arslanagic, R.W. Ziolkowski, O.B. Breinbjerg, Excitation of an electrically small metamaterial-coated cylinder by an arbitrarily located line source. Microw. Opt. Technol. Lett. **48**(12), 2598–2606 (2006). doi:10.1002/mop.21990
15. M.Z. Ghaffar, A.S.Majeed Yaqoob et al., Scattering of electromagnetic wave from perfect electromagnetic conductor cylinders placed in un-magnetized isotropic plasma medium. Optik **125**(17), 4779–4783 (2014). doi:10.1016/j.ijleo.2014.04.061
16. V.L. Ginzburg, *The Propagation of Electromagnetic Waves in Plasmas* (Pergamon Press, New York, 1970), pp. 63–83
17. S.M. Hussain, N.M.Mirza Mirza et al., Beta-efficiency of a typical gas-flow ionization chamber using GEANT4 Monte Carlo simulations. Nucl. Technol. Radiat. **26**(3), 193–200 (2011). doi:10.2298/NTRP1103193H
18. S. Saghamanesh, A. Karimian, M. Abdi, Absorbed dose assessment of cardiac and other tissues around the cardiovascular system in brachytherapy with ^{90}Sr/^{90}Y source by Monte Carlo simulation. Radiat. Prot. Dosim. **147**, 296–299 (2011). doi:10.1093/rpd/ncr347
19. A. Ho, S.S.H. Witharana, G. Jonkmans et al., Detection of bremsstrahlung radiation of ^{90}Sr–^{90}Y for emergency lung counting. Radiat. Prot. Dosim. **151**, 443–449 (2012). doi:10.1093/rpd/ncs029
20. A.A. Kriss, D.M. Hamby, Beta spectroscopy with a large-area avalanche photodiode module and a plastic scintillator. Nucl. Instrum. Methods **A525**, 553–559 (2004). doi:10.1016/j.nima.2004.02.016
21. Bethesda. Average energy required to produce an ion pair, ICRU, ICRU 31, 1997
22. V.D. Zvorykin, A.A. Lonin, A.O. Levchenko et al., Effects of picoseconds terawatt UV laser beam filamentation and a repetitive pulse train on creation of prolonged plasma channels in atmospheric air. Nucl. Instrum. Methods B **309**, 218–222 (2013). doi:10.1016/j.nimb.2013.02.030
23. F. He, C.L. Liu, Studies on fluid model for numerical simulation of gas discharges in color plasma displays. Nucl. Sci. Tech. **2**, 120–125 (2005)
24. W. Liu, J.Z. Zhu, C. Cui et al., Influence of plasma induced by radionuclide layer on the radar cross section of spherical objects. Nucl. Sci. Tech. **26**(4), 040502 (2015). doi:10.13538/j.1001-8042/nst.26.040502
25. H. Jiang, X. Han, R. Li, Improved algorithm for electromagnetic scattering of plane waves by a radially stratified tilted cylinder and its application. Opt. Commun. **26**(4), 13–18 (2006). doi:10.1016/j.optcom.2006.04.041
26. W.J. Lentz, Generating Bessel functions in Mie scattering calculations using continued fractions. Appl. Opt. **15**(3), 668–671 (1976). doi:10.1364/AO.15.000668
27. L. Kai, A. D'Alessio, Finely stratified cylinder model for radially inhomogeneous cylinders normally irradiated by electromagnetic plane waves. Appl. Opt. **34**(24), 5520–5530 (1995). doi:10.1364/AO.34.005520
28. K. Goto, L.H. Loc, Aymptotic solutions for scattered field by a coated conducting cylinder. IEICE Electron. Express **10**(6), 1–10 (2013). doi:10.1587/elex.10.20130139
29. G.T. Ruck, D.E. Barrick, W.D. Stuart, *Radar Cross Section Handbook* (Plenum Press, New York, 1970)
30. I.A. Kotelnikov, G.V. Stupakov, Electromagnetic surface waves on a conducting cylinder. Phys. Lett. A **379**, 1187–1195 (2015). doi:10.1016/j.physleta.2015.02.013
31. W.J. Wiscombe, Improved Mie scattering algorithms. Appl. Opt. **19**(9), 1505–1509 (1980). doi:10.1364/AO.19.001505